*Environ. Sci. Technol.* **2004**, *38*, 746−752

# Modeling the Oxidative Capacity of the Atmosphere of the South Coast Air Basin of California. 1. Ozone Formation Metrics

ROBERT J. GRIFFIN,*,† MEGHAN K. REVELLE,‡,§ AND DONALD DABDUB||

*Department of Civil and Environmental Engineering and Pratt School of Engineering Summer Research Experience for Undergraduates Program, Duke University, Durham, North Carolina 27708, Institute for the Study of Earth, Oceans, and Space and Department of Earth Sciences, University of New Hampshire, Durham, New Hampshire 03824, Department of Computer Science, Mary Washington College, Fredericksburg, Virginia 22401, and Department of Mechanical and Aerospace Engineering, University of California, Irvine, California 92697*

Metrics associated with ozone ($O_3$) formation are investigated using the California Institute of Technology (CIT) three-dimensional air-quality model. Variables investigated include the $O_3$ production rate ($P(O_3)$), $O_3$ production efficiency (OPE), and total reactivity (the sum of the reactivity of carbon monoxide (CO) and all organic gases that react with the hydroxyl radical). Calculations are spatially and temporally resolved; surface-level and vertically averaged results are shown for September 9, 1993 for three Southern California locations: Central Los Angeles, Azusa, and Riverside. Predictions indicate increasing surface-level $O_3$ concentrations with distance downwind, in line with observations. Surface-level and vertically averaged $P(O_3)$ values peak during midday and are highest downwind; surface $P(O_3)$ values are greater than vertically averaged values. Surface OPEs generally are highest downwind and peak during midday in downwind locations. In contrast, peaks occur in early morning and late afternoon in the vertically averaged case. Vertically averaged OPEs tend to be greater than those for the surface. Total reactivities are highest in upwind surface locations and peak during rush hours; vertically averaged reactivities are smaller and tend to be more uniform temporally and spatially. Total reactivity has large contributions from CO, alkanes, alkenes, aldehydes, unsubstituted monoaromatics, and secondary organics. Calculations using estimated emissions for 2010 result in decreases in $P(O_3)$ values and reactivities but increases in OPEs.

## Introduction

Ozone ($O_3$), a respiratory irritant and reactive oxidant, forms in the troposphere as a result of the complex chemistry involving volatile organic compounds (VOCs) and oxides of nitrogen ($NO_x$ = nitrogen oxide (NO) + nitrogen dioxide ($NO_2$)) (*1*). $O_3$ production is initiated by reactions that generate $HO_x$ radicals (hydroxyl (OH), hydroperoxy ($HO_2$), and organic peroxy ($RO_2$)). OH oxidizes VOCs to form $RO_2$ and $HO_2$, which convert NO to $NO_2$. $NO_2$ photolyzes to form an oxygen atom, which combines with molecular oxygen to form $O_3$. Under conditions of high VOC and low $NO_x$ levels, the concentration of $HO_x$ radicals is insensitive to $NO_x$ because the removal of $HO_x$ occurs via $HO_x-HO_x$ reactions. As $NO_x$ increases, the $O_3$ production rate ($P(O_3)$) increases approximately linearly with $NO_x$. At high-$NO_x$ levels, $HO_x-NO_x$ reactions dominate $HO_x$ removal (e.g., to form nitric acid, $HNO_3$). In this regime, $O_3$ production decreases as $NO_x$ increases due to increasingly effective $HO_x$ removal. As a result of this nonlinearity, a change in $NO_x$ or VOCs does not necessarily lead to a similar response in peak $O_3$ (*2*).

Several metrics are used in this study to investigate $O_3$ dynamics within the South Coast Air Basin of California (SoCAB). $P(O_3)$ indicates the rapid nature of $O_3$ formation under peak photochemical conditions and the relative importance of transport and chemistry to peaks in $O_3$ mixing ratios (*3*, *4*). The $O_3$ production efficiency (OPE) compares the $P(O_3)$ to the rate of loss of $NO_x$ (*4*−*6*), illustrating the number of molecules of $O_3$ that are formed per molecule of $NO_x$ emitted. The reactivity of carbon monoxide (CO) or a reactive organic gas (ROG) is defined as the concentration of that species times its reaction rate constant with OH and gives an indication of the compound's ability to form $HO_2$ or $RO_2$ (*3*).

While studies have performed simulations of $O_3$ formation in the SoCAB (*7*−*12*), this is the first to investigate these metrics for the SoCAB. Early work considered metrics in Colorado to estimate averages over the United States and the Northern Hemisphere (*13*), but the majority of other studies have used such calculations to describe air quality in the southeastern United States (*3*, *5*, *6*, *14*−*19*). The study of Kleinman et al. (*3*) also investigated $O_3$ formation metrics in New York City, Phoenix, Philadelphia, and Houston; recent work of Ryerson et al. (*20*) also focused on Houston. Seasonal variations of OPE at Harvard Forest in Massachusetts have also been studied (*21*). Additional recent work by Ryerson et al. (*22*, *23*) focused on calculation of $O_3$ formation metrics in power plant plumes. These studies use observed concentrations of $O_3$, CO, $NO_x$, and VOCs, as opposed to a three-dimensional model, to approximate $O_3$ formation metrics. Data from these studies are compared to the SoCAB results.

## Methodology

The California Institute of Technology (CIT) three-dimensional atmospheric chemical transport model is used to simulate air quality in the SoCAB. The CIT model tracks spatial and temporal distributions of pollutants in 5 km × 5 km horizontal grid cells in each of five vertical layers up to a height of 1.1 km. Application of the CIT model is well-documented (*7*, *8*, *24*, *25*). The current version of the CIT model utilizes the Caltech Atmospheric Chemistry Mechanism (CACM) (*11*), which was developed to predict con-

* Corresponding author phone: (603) 862-2021; Fax: (603) 862-2124; e-mail: rjg@gust.sr.unh.edu.

† Department of Civil and Environmental Engineering, Duke University, and Institute for the Study of Earth, Oceans, and Space and Department of Earth Sciences, University of New Hampshire.

‡ Pratt School of Engineering Summer Research Experience for Undergraduates Program, Duke University, and Department of Computer Science, Mary Washington College.

§ Current address: Department of Computer Science, The College of William and Mary, Williamsburg, VA 23187.

|| University of California at Irvine.



10.1021/es0341283 CCC: $27.50 © 2004 American Chemical Society
Published on Web 12/23/2003

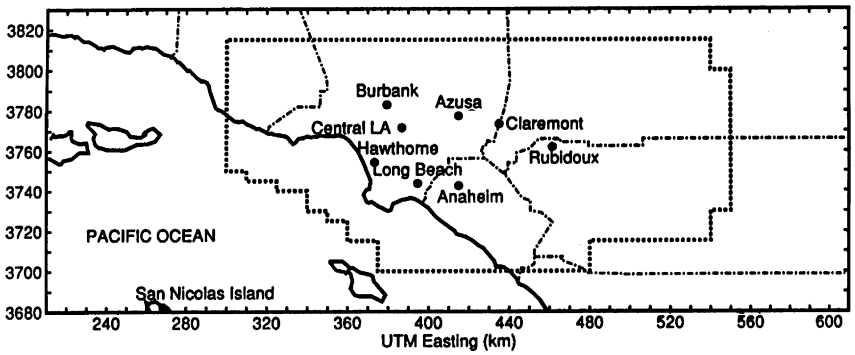


**FIGURE 1. South Coast Air Basin of California showing Central Los Angeles, sampling locations during the 1993 smog episode, and other suburbs for reference. Riverside is less than 5 miles to the southeast of Rubidoux.**

centrations of semivolatile organic oxidation products for use in a module to simulate secondary organic aerosol (SOA) while simultaneously including state-of-the-art treatment of $O_3$ formation.

The atmospheric convective diffusion equation determines the concentration or mixing ratio, $C_i$, of a species $i$ at a given location and time ($t$) (*7*):

$$\frac{\partial C_i}{\partial t} + \nabla\cdot(\bar{\boldsymbol{V}}\boldsymbol{C_i}) = \nabla\cdot(\mathbf{K}\nabla C_i) + F_i + S_i \qquad (1)$$

where $\bar{\boldsymbol{V}}$ is the temporally resolved mean wind velocity vector, $\mathbf{K}$ is the temporally resolved turbulent diffusivity tensor, $F_i$ is the rate of formation (or removal) of species $i$ by gas-phase reactions, and $S_i$ is a source term for emissions. In the current work, all emissions are treated as if they occur at ground level. This assumption affects $O_3$ formation metrics in surface-level cells but becomes less important when values are averaged vertically. Boundary conditions for the solution of eq 1 include a no-flux condition at the top of the modeling domain and the source at the surface being the difference between emission and deposition rates. Harley et al. (*7*) describe the deposition module used in the CIT model. Lateral boundary conditions and initial conditions are established using measured ambient data. The concentrations determined through the solution of eq 1 are used to calculate hourly $O_3$ formation metrics in the SoCAB.

From August 28 to September 13, 1993, a monitoring campaign was performed to identify individual organic species in both the gas and aerosol phases in the SoCAB, which is shown in Figure 1 (*26*). Data from September 8−9, 1993 are used in this investigation of $O_3$ formation metrics. The baseline emissions inventories were generated by the South Coast Air Quality Management District (SCAQMD) as a part of the 1997 Air Quality Management Plan. The biogenics emissions inventory was developed for the late August episode of the South Coast Air Quality Study of 1987. It is assumed that the amount and type of vegetation did not change significantly between the two time periods. Mobile source emissions were generated through use of the California Air Resources Board (CARB) emissions model EMFAC-7G (available at http://www.arb.ca.gov/msei/mvei/mvei/htm). Relevant organic gas-phase emissions are lumped according to chemical structure and property. While more recent versions of the EMFAC model estimate higher mobile source emissions, previous work has shown that on-road motor vehicle emissions in the SoCAB are most likely underpredicted significantly by the methodology used (*27*). Therefore, hot exhaust emissions of VOCs and CO from light duty vehicles were increased by a factor of 3.0 (*7, 28*).

During the smog episode, the SoCAB was subject to a high-pressure meteorological system characterized by a strong temperature inversion aloft and sunny and hot conditions, limiting vertical mixing and intensifying photochemistry. Hourly surface wind speed and direction observations were taken by the California Irrigation Management Information Service (CIMIS) and SCAQMD at a combined 53 sites. CIMIS, SCAQMD, and the National Climatic Data Center recorded temperature and relative humidity at a combined 86 sites. Total solar radiation was monitored at a combined 27 sites by SCAQMD and CIMIS. Ultraviolet radiation was measured in Central Los Angeles (CELA) by SCAQMD. The methodology described in Harley et al. (*7*) was used to generate hourly gridded meteorological fields. Inversion base height and wind aloft were inferred from upper air measurements made daily by SCAQMD in West Los Angeles and CARB in Claremont. The method of Winner and Cass (*29*) was used for creating mixing depth fields from these data.

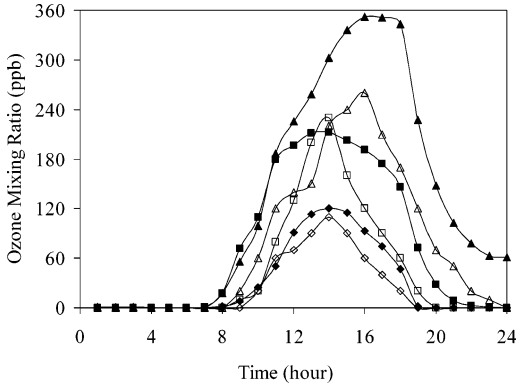


**FIGURE 2. Simulated (filled symbols) versus observed (open symbols) surface-level $O_3$ mixing ratios for September 9, 1993 in CELA (diamonds), AZUS (squares), and RIVR (triangles).**

Gas-phase species including $NO_x$, $O_3$, and CO were monitored hourly by SCAQMD at numerous monitoring sites throughout the SoCAB. Such data have been used to validate the performance of the CIT model and CACM (*11, 12*). Simulated versus observed surface-level $O_3$ mixing ratios for CELA, Azusa (AZUS), and Riverside (RIVR) on September 9, 1993 are shown in Figure 2. The CIT model is initialized on the afternoon of September 7, 1993. By showing output from September 9, any bias associated with initial conditions is minimized. The locations displayed in Figure 2 represent different characteristic regions of the SoCAB. Primary emissions dominate in CELA due to proximity to the hub of the region's freeway system. AZUS and RIVR are downwind (dominant wind patterns are west to east) locations typified by secondary photochemical activity and transport of pollutants from upwind locations.

Figure 2 indicates that the CIT model matches the temporal distribution of $O_3$ concentrations. While peak $O_3$ concentrations are predicted within 10% for CELA (over) and AZUS (under), peak $O_3$ concentrations in RIVR are overpre-

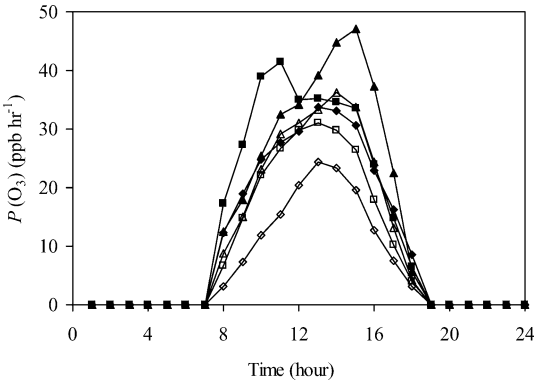


**FIGURE 3. Simulated $P(O_3)$ values on September 9, 1993 in CELA (diamonds), AZUS (squares), and RIVR (triangles). Filled symbols represent surface cell values, while open symbols indicate vertically averaged values.**

dicted by 35%, due to uncertainty in the emissions profiles, the chemical mechanism, the transport mechanism, and meteorological inputs (*11*). The level of consistency between observations and simulations in this model is consistent with previous studies (*7*, *30*, *31*). Figure 2 also shows that peak $O_3$ mixing ratios and the hour at which they occur increase in the downwind direction. It should be noted that the CIT model has not been adjusted to attempt to better match $O_3$ simulations to observations in an effort to meet Environmental Protection Agency model performance guidelines (http://www.epa.gov/scram001/guidance/guide/drafto3.pdf). Instead, the model is used as a diagnostic tool to identify where the best available knowledge and/or data are not leading to a high level of model performance, as in RIVR. The overprediction of peak $O_3$ in RIVR may also lead to overprediction of the metrics presented here.

## Results and Discussion

***P*(O₃).** $P(O_3)$ (ppb $h^{-1}$) is the instantaneous rate of reaction leading to $O_3$ formation and indicates how quickly precursors are chemically converted to $O_3$. In a $NO_x$-rich environment such as the SoCAB (*32*), $P(O_3)$ is estimated by (*3*):

$$P(O_3) = k_{CO,OH}[CO][OH] + \sum_i k_{i,OH} Y_i [ROG_i][OH] \quad (2)$$

where $k_{i,OH}$ ($ppb^{-1}$ $h^{-1}$) represents the kinetic rate constant for the reaction between OH and species $i$, $Y_i$ represents the stoichiometric yield of peroxy radicals in the reaction between OH and ROG species $i$, and the bracket notation represents mixing ratios (ppb). This expression assumes that the rate-limiting step in $O_3$ formation is the oxidation of ROGs or CO to form $RO_2$ and/or $HO_2$. Although some oxidation of ROGs and CO occurs without sunlight because OH is nonzero at night, $P(O_3)$ values between dusk and dawn are forced to zero because of negligible rates of $NO_2$ photolysis. Previous studies have defined $P(O_3)$ as the rate of reaction between NO and peroxy radicals (*6*). Use of this methodology yields slightly higher values than those presented here.

$P(O_3)$ values (surface-level and vertically averaged) calculated with the CIT model for the three locations of interest are shown as a function of time in Figure 3. Vertical averages are a weighted average based upon the fraction that each vertical level contributes to the total model vertical domain. In comparison to $O_3$ mixing ratios, $P(O_3)$ values are somewhat more homogeneous spatially yet tend to also be slightly higher downwind. Peak $P(O_3)$ values for the three locations range from 33.8 to 47.0 ppb $h^{-1}$ for surface values and from 23.4 to 36.3 ppb $h^{-1}$ for vertically averaged values. Peaks occur during midday (1100−1500 h) when photochemical activity is highest.

Figure 4 exhibits the temporal and spatial distribution of vertically averaged $P(O_3)$ values within the SoCAB. The top of Figure 4 shows a contour of $P(O_3)$ in the SoCAB at 1100 h; correspondingly the bottom shows a contour of $P(O_3)$ at 1500 h. Figure 4 indicates that $P(O_3)$ values are highest within the central corridor of the SoCAB between CELA and RIVR, that maximum $P(O_3)$ are less than 50 ppb $h^{-1}$, and that the peak $P(O_3)$ values move downwind and diffuse as time increases, as would be expected.

Estimates of $P(O_3)$ for other locations are typically calculated from airplane-based measurements. In addition, the episode modeled here exhibited some of the worst air quality in the SoCAB for 1993. Therefore, a comparison of the vertically averaged $P(O_3)$ values simulated here to peak $P(O_3)$ values in other locations is warranted. Typical peak $P(O_3)$ values as high as approximately 50, 50, 30, and 200 ppb $h^{-1}$ were estimated for the summer of 1999 in Philadelphia, the summer of 1999 in Nashville, the late spring of 1998 in Phoenix, and the summer of 2000 in Houston, respectively (*3*, *17*, *18*). The largest values exhibited for Houston represent samples taken in the Houston Ship Channel; a more representative peak $P(O_3)$ value for metropolitan Houston is 40 ppb $h^{-1}$. The 90th percentile $P(O_3)$ values for these locations at these times were 22.3, 15.2, 7.6, and 39.1 ppb $h^{-1}$, respectively. The 90th percentile $P(O_3)$ for New York City during July of 1996 was 14.7 ppb $h^{-1}$ (*3*). At a rural site in eastern Georgia, $P(O_3)$ values were less than 30 ppb $h^{-1}$ (*15*). Data presented in this study indicate that the SoCAB experiences peak $P(O_3)$ values on par with other urban areas in the continental United States, particularly Philadelphia, Nashville, and Houston.

**OPE.** The OPE (dimensionless) is defined as:

$$\mathrm{OPE} = \frac{P(O_3)}{L(NO_x)} \quad (3)$$

where $L(NO_x)$ (ppb $h^{-1}$) is the rate of loss of $NO_x$, which does not consider $NO_x$ interconversion reactions; only reactions that consume NO or $NO_2$ and lead to other slower reacting N-containing products such as $HNO_3$ and nitroorganics are considered in $L(NO_x)$. Formation of fast-reacting N-containing species such as the nitrate radical or nitrous acid that cycle very efficiently and quickly back to $NO_x$ during daylight hours is not included (*1*).

Surface-level and vertically averaged OPEs calculated within the CIT model for the three locations of interest are shown as a function of time in Figure 5. OPEs are typically smallest in CELA, particularly during midday (1200 through 1600 h) (midday-averaged and maximum values of 3.2 and 6.2 for surface cells; corresponding vertically averaged values are 5.0 and 12.7). The four corresponding values for AZUS are 4.3, 5.1, 4.7, and 18.2. RIVR presents values of 5.7, 6.1, 6.4, and 9.3. For surface-level values, OPE maxima in downwind locations occur during peak photochemical times because of the link to $P(O_3)$. Vertically averaged OPEs, however, show an early morning peak in all three locations. Given the low $P(O_3)$ values associated with early morning and late afternoon, the $L(NO_x)$ values in upper levels of the model at these times must be extremely small to account for this peak in OPE. Because $L(NO_x)$ is controlled primarily by OH and $NO_2$ (leading to $HNO_3$) and because $P(O_3)$ is linear in OH, the concentration of $NO_2$ must therefore be very small in the upper levels of the model at these times. In the early morning, upper-level concentrations of $NO_2$ are low as a result of low vertical mixing and a lack of photochemistry overnight. Late afternoon peaks in vertically averaged OPE must also result from small upper-level $NO_2$ mixing ratios. Given that OPEs over the continental United States range from 1 to 20 (*4*), OPEs in the SoCAB are on the small side, indicating efficient removal of $NO_x$ due to a $NO_x$-rich environment. The higher

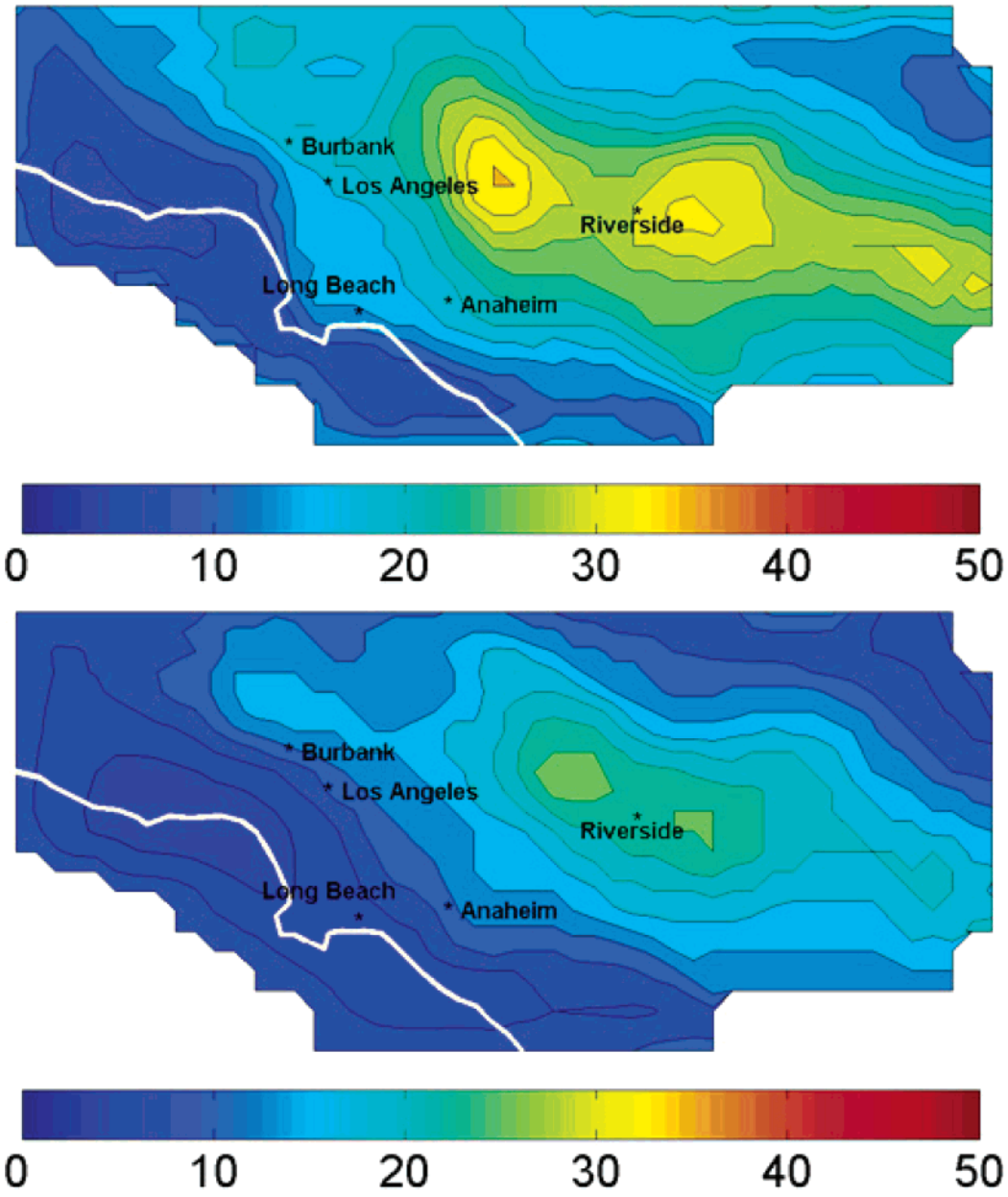


**FIGURE 4. Simulated vertically averaged $P(O_3)$ values (ppb $h^{-1}$) as a function of location in the SoCAB at 1100 (top) and 1500 h (bottom).**

downwind and vertically averaged OPE values exhibited in the current work confirm the recent work of Ryerson et al. (*22*, *23*) that showed higher OPE values in a less concentrated power plant plume.

Vertically and temporally (midday, 1200−1600 h) averaged values (range of 4.7−6.4) are used for comparative purposes. Slightly higher average OPEs (up to 10) were observed in urban and rural locations in the southeastern United States during summers in the early and mid-1990s (*5*, *6*, *14*, *16*, *17*), most likely because the atmosphere of the southeastern United States tends to be more limited by $NO_x$ availability. OPEs estimated for Harvard Forest in rural Massachusetts over the summers of 1990 to 1994 range from 2 to 8, depending on the calculation method used (*21*). Observations in the Houston urban plume during the summer of 2000 lead to an estimate for OPE of 5.4 (*20*), a number within the range of averages presented here for the SoCAB.

**Total Reactivity.** How quickly a species reacts with OH indicates potential for $O_3$ formation because such reactions lead to radicals that convert NO to $NO_2$. The reactivity, $R_j$ ($s^{-1}$), of species $j$ is defined by the product of its concentration and its kinetic rate constant for oxidation by OH. Total reactivity, $R$ ($s^{-1}$), is the sum of the individual reactivities:

$$R = \sum_j R_j = k_{CO,OH}[CO] + \sum_i k_{ROG_i,OH}[ROG_i] \qquad (4)$$

Surface-level and vertically averaged total reactivities calculated using the CIT model are shown in Figure 6 for September 9, 1993 in the three locations of interest. Surface-level total reactivity is highest in upwind locations and peaks during both the morning and evening rush hours. In CELA, the surface-level daylight-averaged total reactivity is 103.0 $s^{-1}$, with a maximum of 230.0 $s^{-1}$ occurring at 0800 h. The surface-level daylight-averaged total reactivity in AZUS is 67.9 $s^{-1}$, with a maximum of 119.3 $s^{-1}$ occurring at 0800 h. The corresponding values in RIVR are 46.7 and 62.8 $s^{-1}$, respectively. The maximum total reactivity in RIVR also occurs at 0800 h. Higher reactivities occur outside the range of strong daylight in both AZUS and RIVR. When vertically averaged, the daylight-averaged reactivity in CELA is 33.6 $s^{-1}$ while the peak of 41.9 $s^{-1}$ occurs at 0900 h. AZUS presents corre-

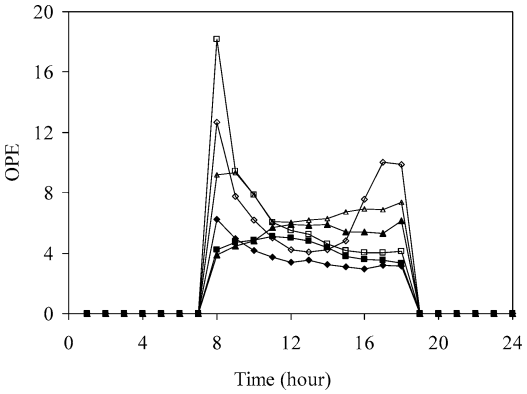


**FIGURE 5. Simulated OPEs on September 9, 1993 in CELA (diamonds), AZUS (squares), and RIVR (triangles). Filled symbols represent surface cell values, while open symbols indicate vertically averaged values.**

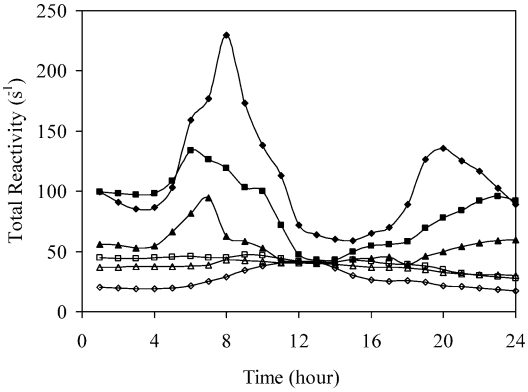


**FIGURE 6. Simulated total reactivity values on September 9, 1993 in CELA (diamonds), AZUS (squares), and RIVR (triangles). Filled symbols represent surface cell values, while open symbols indicate vertically averaged values.**

sponding values of 42.8 and 47.2 $s^{-1}$ at 0900 h; the values for RIVR are 39.6 and 43.0 $s^{-1}$ at 0800 h, respectively. Vertically averaged reactivities are more spatially and temporally uniform than surface-level values.

Kleinman et al. (*3*) show average total reactivity values when the $P(O_3)$ is above the 90th percentile in Nashville, New York City, Phoenix, Philadelphia, and Houston that are smaller than those calculated for the SoCAB during the 1993 episode (vertically and daylight-averaged range of 33.6−42.8 $s^{-1}$). The values presented for other cities are consistent with recent estimates by Kovacs et al. (*19*) and Ryerson et al. (*20*) for Nashville and Houston, respectively. The averaged value presented for Houston when $P(O_3)$ is above the 90th percentile (approximately 25 $s^{-1}$) is by far the closest to the averaged values calculated for CELA, AZUS, and RIVR. The consistency between the SoCAB and Houston and the discrepancies between the SoCAB and the remaining cities are intuitive because the SoCAB and Houston are traditionally the metropolitan areas in the nation with the worst air quality. However, it is striking that these values are so similar. The SoCAB is dominated by typical urban emissions from motor vehicles and is characterized by low mixing layer heights and topography that traps pollutants. Houston is characterized by similar motor vehicle emissions but dominated by an extremely large petrochemical industry not present in the SoCAB.

**Individual Species Reactivity.** The contribution of individual species to vertically averaged total reactivity at 1100 and 1500 h in each of the three locations is shown in Figure 7, as is the percent contribution. Species considered include CO, methane, alkanes, formaldehyde (HCHO), higher aldehydes, alcohols, nonbiogenic alkenes, ketones, isoprene, functional monoaromatics (such as phenol or nitrotoluene), low- and high- SOA yield unsubstituted (except for alkyl groups) monoaromatics (*33*), monoterpenes, polycyclic aromatic hydrocarbons (PAH), and polyfunctional secondary organic oxidation products that cannot be solely classified as part of any of the previous groups (for example, keto-aldehydes). In the earlier part of the day, individual species generally have higher reactivities in upwind locations compared to downwind locations. Aldehydes are an exception, which implies that the secondary formation of these aldehydes is an important process. Secondary species cause a larger difference between upwind and downwind locations later in the day. Parts c and d show that the percent contributions of individual species to reactivity are relatively constant from upwind to downwind locations with the exception of alkenes and high- and low-yield aromatics, which decrease in the downwind direction, and higher aldehydes, which increase.

For July 11, 1995, Daum et al. (*17*) show that anthropogenic hydrocarbons and CO contributed approximately two-thirds of the total OH reactivity in Nashville; biogenic compounds play a much larger role in atmospheric chemistry in Nashville compared to the SoCAB. Kleinman et al. (*3*) indicate that CO, HCHO, biogenic hydrocarbons, and anthropogenic hydrocarbons dominate reactivity in Nashville, New York City, Philadelphia, Phoenix, and Houston when the $P(O_3)$ is greater than the 90th percentile. CO and HCHO reactivity are fairly consistent when comparing these five cities and the SoCAB, though the CO reactivity is predicted to be slightly larger in the SoCAB, potentially because of inflated emissions estimates and limited vertical mixing. There is a wide range in the contribution of biogenic and anthropogenic organics to reactivity. In Nashville and New York City, the contribution of biogenic precursors is greater than that of anthropogenic precursors. In Philadelphia, the contribution from the two groups appears to be approximately the same. In Phoenix, the anthropogenic fraction is somewhat more important. As in the SoCAB, anthropogenic species are by far the largest contributor to reactivity in Houston.

**Effect of Emissions on Ozone Metrics.** Because of the large uncertainties associated with emissions estimates, the effect on $O_3$ formation metrics of changes in emissions is investigated. Emissions estimates for 2010 for the SoCAB are used for this purpose. The 2010 emissions inventory is based on the best-estimate emissions of the SCAQMD and is derived similarly to those for 1993. In the SoCAB, the total emission rates decrease from 2404 to 981 metric tons $day^{-1}$ for VOCs, from 867 to 407 metric tons $day^{-1}$ for $NO_x$, and from 12 249 to 3268 metric tons $day^{-1}$ for CO. Emissions decrease in the individual locations as well, as shown in Table 1.

For the three locations of interest, Table 1 presents peak modeled surface-level $O_3$ mixing ratios using the 1993 meteorology and 2010 emissions. It must be noted that the 1993 meteorology is very favorable for $O_3$ formation. A 14.6% increase in peak $O_3$ is predicted in CELA while decreases in peak $O_3$ of 5.1 and 27.2% are predicted for AZUS and RIVR, respectively. The increase in CELA is due to the nonlinearity of $O_3$ formation chemistry in response to decreases in VOC and $NO_x$ discussed in the Introduction.

Also presented in Table 1 is a comparison of vertically averaged simulated $O_3$ formation metrics in the three locations of interest. Average and peak $P(O_3)$ values decrease on average by a factor 1.8; even stronger reductions (average factor of 2.7) are estimated for reactivity. These reductions result directly from large decreases in CO and VOC emissions between 1993 and 2010. When emissions are reduced, OPE values increase on average by a factor of 1.2. These results are in accord with those of Ryerson et al. (*22, 23*) that indicated higher OPEs in less concentrated plumes. Vertically averaged

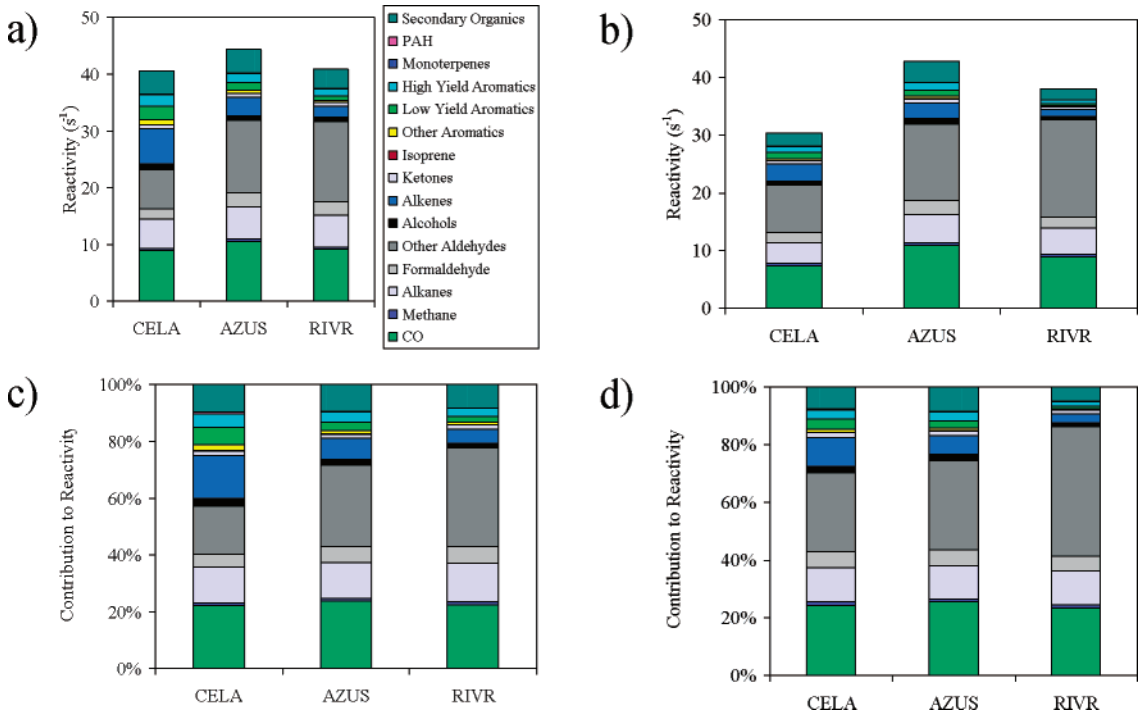


**FIGURE 7. Contribution of individual species to vertically averaged total reactivity: (a) 1100 h; (b) 1500 h; (c) percent contribution at 1100 h; (d) percent contribution at 1500 h.**

**TABLE 1. Comparison of Site-Specific Emissions, Peak Modeled Surface $O_3$ Mixing Ratios, and Modeled Peak and Temporally Averaged $O_3$ Formation Metrics between 1993 and 2010[a]**

| | for given year | | | | | |
|---|---|---|---|---|---|---|
| | CELA | | AZUS | | RIVR | |
| | 1993 | 2010 | 1993 | 2010 | 1993 | 2010 |
| CO emissions (kg day$^{-1}$) | 107 036 | 11 507 | 34 551 | 5 526 | 19 851 | 5 464 |
| VOC emissions (kg day$^{-1}$) | 16 314 | 2 569 | 5 733 | 1 227 | 3 692 | 1 286 |
| $NO_x$ emissions (kg day$^{-1}$) | 8 919 | 1 269 | 2 564 | 761 | 1 431 | 1 132 |
| peak $O_3$ (ppb) | 120.2 | 137.8 | 212 | 201.2 | 351.6 | 255.8 |
| peak $P(O_3)$ (ppb h$^{-1}$) | 24.3 (1300) | 12.5 (1300) | 31.1 (1300) | 17.5 (1300) | 36.3 (1400) | 20.1 (1400) |
| av $P(O_3)$ (ppb h$^{-1}$) | 13.5 | 7.9 | 20.0 | 10.5 | 22.9 | 12.3 |
| peak OPE | 12.7 (0800) | 13.4 (0800) | 18.2 (0800) | 22.3 (0800) | 9.3 (0900) | 17.2 (0800) |
| av OPE | 5.0 | 5.3 | 4.7 | 5.1 | 6.4 | 5.9 |
| peak $R$ (s$^{-1}$) | 41.8 (1200) | 13.0 (1000) | 47.2 (0900) | 17.4 (1000) | 43.0 (0800) | 18.2 (1100) |
| av $R$ (s$^{-1}$) | 33.6 | 11.6 | 42.8 | 15.4 | 39.6 | 17.2 |

[a] Metric values reflect vertical averages, and temporal averages for $P(O_3)$ and $R$ include only those times when $P(O_3)$ values are nonzero. Temporal averages for OPEs represent midday (1200−1600 h). The timing of the peak of the metric is also noted. Note that the overall maximum reactivity may have occurred outside of the included hours.

OPEs for the 2010 scenario still exhibit early morning and late afternoon peaks.

Besides the biogenic species, every species considered has a decreased absolute reactivity in the 2010 scenario compared to that of 1993. The increase in reactivity of the biogenics is linked to improved emissions inventories that predict larger emissions rates. In addition, increases in biogenic reactivity may result from less consumption of biogenics by $O_3$, the mixing ratio of which typically decreases in downwind locations because of decreased anthropogenic emissions. The relative contribution to total reactivity significantly changes between 1993 and 2010 for only a limited number of species; these changes are consistent between the three locations of interest. The biggest decreases occur for CO and alkenes because of large decreases in their emissions. The largest increases are observed for isoprene and higher aldehydes. Again, isoprene is one of the few species whose absolute individual reactivity increases between the 1993 and the 2010 scenarios. The increase in the relative contribution of aldehydes despite their decrease in absolute individual reactivity is most likely a result of their high reaction rate constant with OH.

## Acknowledgments

The authors thank three anonymous reviewers for invaluable comments, Professor Robert Harley of UC—Berkeley and Dr. Greg Frost of the NOAA Aeronomy Laboratory for helpful discussions, and Marc Carreras of UC—Irvine for help in preparing the 2010 emissions. Support of M.K.R. from the REU Site at the Duke Pratt School of Engineering (sponsored by the National Science Foundation under Grant 0139460) is greatly appreciated. Any opinions, findings, and conclusions or recommendations expressed in this material are those of the authors and do not necessarily reflect the views of the National Science Foundation. The research described in this article has also been funded in part by the United States Environmental Protection Agency through Cooperative Agreement CR829068-01 to the University of Houston. It has not been subjected to the Agency's required peer and policy

review and therefore does not necessarily reflect the views of the Agency, and no official endorsement should be inferred.

## Literature Cited


(1) Seinfeld, J. H.; Pandis, S. N. *Atmospheric Chemistry and Physics from Air Pollution to Climate Change*; Wiley: New York, 1998.
(2) Dodge, M. C. *Atmos. Environ.* **1984**, *18*, 1657.
(3) Kleinman, L. I.; Daum, P. H.; Imre, D.; Lee, Y.-N.; Nunnermacker, L. J.; Springston, S. R.; Weinstein-Lloyd, J.; Rudolph, J. *Geophys. Res. Lett.* **2002**, *29*, 1467 (doi: 10.1029/2001GL014569).
(4) Jacob, D. J. *Introduction to Atmospheric Chemistry*; Princeton University Press: Princeton, NJ, 1999.
(5) Sillman, S.; He, D. Y.; Pippin, M. R.; Daum, P. H.; Imre, D. G.; Kleinman, L. I.; Lee, J. H.; Weinstein-Lloyd, J. *J. Geophys. Res., [Atmos.]* **1998**, *103*, 22629.
(6) Trainer, M.; Ridley, B. A.; Buhr, M. P.; Kok, G.; Walega, J.; Hübler, G.; Parrish, D. D.; Fehsenfeld, F. C. *J. Geophys. Res., [Atmos.]* **1995**, *100*, 18823.
(7) Harley, R. A.; Russell, A. G.; McRae, G. J.; Cass, G. R.; Seinfeld, J. H. *Environ. Sci. Technol.* **1993**, *27*, 378.
(8) Meng, Z.; Dabdub, D.; Seinfeld, J. H. *Science* **1997**, *277*, 116.
(9) Lu, R.; Turco, R. P. *Atmos. Environ.* **1996**, *30*, 4155.
(10) Lu, R.; Turco, R. P.; Jacobson, M. Z. *J. Geophys. Res., [Atmos.]* **1997**, *102*, 6081.
(11) Griffin, R. J.; Dabdub, D.; Seinfeld, J. H. *J. Geophys. Res., [Atmos.]* **2002**, *107*, 4332 (doi: 10.1029/2001JD000541).
(12) Griffin, R. J.; Dabdub, D.; Kleeman, M. J.; Fraser, M. P.; Cass, G. R.; Seinfeld, J. H. *J. Geophys. Res., [Atmos.]* **2002**, *107*, 4334 (doi: 10.1029/2001JD000544).
(13) Liu, S. C.; Trainer, M.; Fehsenfeld, F. C.; Parrish, D. D.; Williams, E. J.; Fahey, D. W.; Hübler, G.; Murphy, P. C. *J. Geophys. Res., [Atmos.]* **1987**, *92*, 4191.
(14) Olszyna, K. J.; Bailey, E. M.; Simonaitis, R.; Meagher, J. F. *J. Geophys. Res., [Atmos.]* **1994**, *99*, 14557.
(15) Kleinman, L. I.; Lee, Y.-N.; Springston, S. R.; Lee, J. H.; Nunnermacker, L.; Weinstein-Lloyd, J.; Zhou, X.; Newman, L. *J. Geophys. Res., [Atmos.]* **1995**, *100*, 7263.
(16) Nunnermacker, L. J.; Imre, D.; Daum, P. H.; Kleinman, L.; Lee, Y.-N.; Lee, J. H.; Springston, S. R.; Newman, L.; Weinstein-Lloyd, J.; Luke, W. T.; Banta, R.; Alvarez, R.; Senff, C.; Sillman, S.; Holdren, M.; Keigley, G. W.; Zhou, X. *J. Geophys. Res., [Atmos.]* **1998**, *103*, 28129.
(17) Daum, P. H.; Kleinman, L. I.; Imre, D.; Nunnermacker, L. J.; Lee, Y.-N.; Springston, S. R.; Newman, L.; Weinstein-Lloyd, J.; Valente, R. J.; Imhoff, R. E.; Tanner, R. L.; Meagher, J. F. *J. Geophys. Res., [Atmos.]* **2000**, *105*, 9107.
(18) Thornton, J. A.; Wooldridge, P. J.; Cohen, R. C.; Martinez, M.; Harder, H.; Brune, W. H.; Williams, E. J.; Roberts, J. M.; Fehsenfeld, F. C.; Hall, S. R.; Shetter, R. E.; Wert, B. P.; Fried, A. *J. Geophys. Res., [Atmos.]* **2002**, *107*, 4146 (doi: 10.1029/2001JD000932).
(19) Kovacs, T. A.; Brune, W. H.; Harder, H.; Martinez, M.; Simpas, J. B.; Frost, G. J.; Williams, E.; Jobson, T.; Stroud, C.; Young, V.; Fried, A.; Wert, B. *J. Environ. Monit.* **2003**, *5*, 68.
(20) Ryerson, T. B.; Trainer, M.; Angevine, W. M.; Brock, C. A.; Dissly, R. W.; Fehsenfeld, F. C.; Frost, G. J.; Goldan, P. D.; Holloway, J. S.; Hübler, G.; Jakoubek, R. O.; Kuster, W. C.; Neuman, J. A.; Nicks, D. K., Jr.; Parrish, D. D.; Roberts, J. M.; Sueper, D. T.; Atlas, E. L.; Donnelly, S. G.; Flocke, F.; Fried, A.; Potter, W. T.; Schauffler, S.; Stroud, C.; Weinheimer, A. J.; Wert, B. P.; Wiedinmyer, C.; Alvarez, R. J.; Banta, R. M.; Darby, L. S.; Senff, C. J. *J. Geophys. Res., [Atmos.]* **2003**, *108*, 4249 (doi: 10.1029/2002JD003070).
(21) Hirsch, A. I.; Munger, J. W.; Jacob, D. J.; Horowitz, L. W.; Goldstein, A. H. *J. Geophys. Res., [Atmos.]* **1996**, *101*, 12659.
(22) Ryerson, T. B.; Buhr, M. P.; Frost, G. J.; Goldan, P. D.; Holloway, J. S.; Hübler, G.; Jobson, B. T.; Kuster, W. C.; McKeen, S. A.; Parrish, D. D.; Roberts, J. M.; Sueper, D. T.; Trainer, M.; Williams, E. J.; Fehsenfeld, F. C. *J. Geophys. Res., [Atmos.]* **1998**, *103*, 22569.
(23) Ryerson, T. B.; Trainer, M.; Holloway, J. S.; Parrish, D. D.; Huey, L. G.; Sueper, D. T.; Frost, G. J.; Donnelly, S. G.; Atlas, E. L.; Kuster, W. C.; Goldan, P. D.; Hübler, G.; Meagher, J. F.; Fehsenfeld, F. C. *Science* **2001**, *292*, 719.
(24) Pandis, S. N.; Wexler, A. S.; Seinfeld, J. H. *Atmos. Environ.* **1993**, *27A*, 2403.
(25) Meng, Z.; Dabdub, D.; Seinfeld, J. H. *J. Geophys. Res., [Atmos.]* **1998**, *103*, 3419.
(26) Fraser, M. P.; Grosjean, D.; Grosjean, E.; Cass, G. R. *Environ. Sci. Technol.* **1996**, *30*, 1731.
(27) Pierson, W. R.; Gertler, A. W.; Bradow, R. L. *J. Air Waste Manage. Assoc.* **1990**, *40*, 1495.
(28) Fraser, M. P.; Kleeman, M. J.; Schauer, J. J.; Cass, G. R. *Environ. Sci. Technol.* **2000**, *34*, 1302.
(29) Winner, D. A.; Cass, G. R. *Atmos. Environ.* **1999**, *33*, 431.
(30) Harley, R. A.; Cass, G. R. *Atmos. Environ.* **1995**, *29*, 905.
(31) Jacobson, M. Z.; Lu, R.; Turco, R. P.; Toon, O. B. *Atmos. Environ.* **1996**, *30*, 1939.
(32) Kelly, N. A.; Gunst, R. F. *Atmos. Environ.* **1990**, *24A*, 2991.
(33) Odum, J. R.; Jungkamp, T. P. W.; Griffin, R. J.; Flagan, R. C.; Seinfeld, J. H. *Science* **1997**, *276*, 96.



*Received for review February 12, 2003. Revised manuscript received October 13, 2003. Accepted October 30, 2003.*

ES0341283